

Naturally occurring scour pits in nearshore sands

Alex E. Hay and Rachel Speller

Department of Oceanography, Dalhousie University, Halifax, Nova Scotia, Canada

Received 30 June 2004; revised 20 December 2004; accepted 25 January 2005; published 28 April 2005.

[1] Depressions 10–50 cm in diameter and $O(10)$ cm deep were observed in rotary acoustic imagery of the seafloor during SandyDuck97. The rotary sonar record spans a 77 day period and 13 storm events. The depressions occurred during both the wave growth and the wave decay phases of each storm and over a relatively narrow range of wave energies ($u_{\text{rms}} = 0.32 \text{ cm/s} \pm 0.05 \text{ cm/s}$ standard deviation) and grain roughness Shields parameters ($= 0.7 \pm 0.2$). The observations are mainly from the outer surf zone in ≈ 3 m mean water depth at two stations separated by 40 m cross-shore distance. Depressions were 6.5 times more frequent at the inner station ($N = 485$) than at the outer ($N = 75$). Areal densities were small: $O(0.1) \text{ m}^{-2}$. Depressions were also observed in the inner surf zone at a third station, for which the data record is less complete. The probability distribution of the locations of depression first occurrences is nonrandom (i.e., non-Poisson) due to 50% reoccurrence in roughly the same positions from storm to storm. The geometry and temporal development of the depressions are similar to scour pits formed by cylindrical piles and other objects. On the basis of these similarities, and the clustering of first occurrence locations, we conclude that the likely origin of the depressions is scour about compact semimobile obstacles on or embedded within the sandy seafloor. Possible candidate obstacles include pebbles, large shells or large shell fragments, and the chimney structures left by burrowing organisms. Importantly, 13 of the pits evolved into meter-scale lunate megaripples, indicating that these features can act as megaripple precursors.

Citation: Hay, A. E., and R. Speller (2005), Naturally occurring scour pits in nearshore sands, *J. Geophys. Res.*, *110*, F02004, doi:10.1029/2004JF000199.

1. Introduction

[2] One of the objectives of the SandyDuck97 nearshore dynamics experiment was to investigate the conditions under which different bedstates occur. As shown first by Clifton [1976] and coworkers, a rich but quasi-repeatable variety of bed form types is found in the nearshore zone, including the impressively large and highly three-dimensional lunate megaripple. These latter bed forms, which can be several meters in horizontal scale and half a meter high, had been observed during Duck94 [Gallagher *et al.*, 1998; Ngusaru and Hay, 2004] and were much anticipated in the planning and preparations for SandyDuck97. One of the surprises of the 1997 experiment, therefore, was the relatively small number of times that lunate megaripples made an appearance [Hay and Mudge, 2005]. Instead, curious small depressions were observed in our acoustic imagery of the seafloor, both during storm wave growth and again during wave decay. Occasionally these depressions developed into lunate megaripples. Thus rather than being just a curiosity, the depressions represent a little-studied natural phenomenon with significant implications for nearshore sediment dynamics.

[3] There have been few reports in the literature of naturally occurring scour pits in sandy, wave-dominated environments. In a study of scour around vertical piles in

the nearshore, Palmer [1969] included some results for scour about stones and rocks on a sand substrate. Hill and Hunter [1976] reported pits in the inner surf zone formed by scour around “chimney-structures” created by burrowing shrimp. The great majority of investigations into scour forced by wave action have been in relation to engineering structures [Sumer and Fredsoe, 2002], such as vertical piles, and more recently mine-like objects [Voropayev *et al.*, 2003]. The experimental aspects of these investigations have been mainly carried out in the laboratory.

[4] The purpose of this paper is to address the following questions. (1) What were the hydrodynamic conditions under which scour pits formed during SandyDuck97, and what is their relationship to the occurrence conditions for other bedstates? (2) What were the spatial (geometry and distribution pattern) and temporal (lifetimes and growth rates) characteristics of these scour pits? (3) How do the results from the first two questions relate to the mechanics of scour around known objects? (4) What are the likely origins of the observed scour pits? (5) Under what conditions do scour pits lead to the development of lunate megaripples?

[5] The paper is organized as follows. The instrumentation, methods and definitions of forcing statistics are outlined in section 2. The main experimental results are presented in section 3, beginning with scour pit occurrence in relation to hydrodynamic forcing parameters (section 3.1)

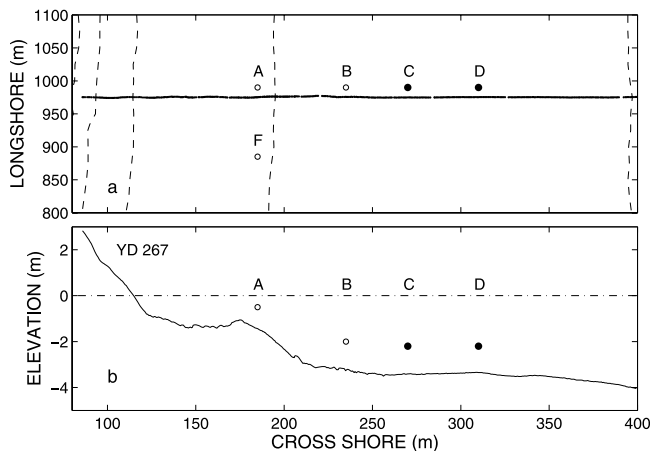


Figure 1. (a) Instrument frame locations. Solid circles indicate frames C and D. Dashed lines are bottom contours (2 m intervals). The solid line is the transect corresponding to the bathymetric profile shown in Figure 1b. (b) Beach profile on 24 September 1997 (year day (YD) 267). The dash-dotted line indicates National Geodetic Vertical Datum (NGVD).

and relative to other bedstates (section 3.2), followed by pit geometric characteristics (section 3.3), and the probability distributions for pit locations (section 3.4) and for pit growth rates (section 3.5). The presence/absence of detectable objects (nuclei) in the pit centers, and the development of lunate megaripples from scour pit precursors, are treated in sections 3.6 and 3.7. In section 4, these results are compared to the characteristics of scour pits in other studies, and several candidate obstacles which might have acted as nuclei for scour pit development at the experiment site are identified. A brief summary and our conclusions are given in section 5.

2. Methods

2.1. Field Experiment

[6] SandyDuck97 (SD97) took place between August and November 1997 at the US Army Corps of Engineers Field Research Facility (FRF) near Duck, North Carolina. The FRF is located on the Outer Banks, a barrier island system along the North Carolina coast, and is described by *Birkemeier et al.* [1985].

[7] The locations of the instrument frames for the component of SD97 discussed here are indicated in Figure 1. The instrument frames are described by *Hay and Mudge* [2005]. Viatran pressure sensors and Marsh-McBirney electromagnetic (EM) flowmeters were mounted on each frame, the EMs at a nominal height above bottom of 35 cm. This height of course changed as the local bed elevation evolved, and the vertical positions of the flowmeters and pressure sensor ports were adjusted from time to time by SCUBA divers to compensate. The EM flowmeters and pressure sensors were sampled at 2 Hz continuously, with records stored at 0.5 hour intervals. (See *Henderson and Bowen* [2002] and *Hay and Mudge* [2005] for further discussion and analysis of the EM and pressure sensor data.)

[8] The bedstate results presented here are based mainly on rotary fan and pencil beam acoustic images acquired at

frames C and D, located 160 m and 200 m offshore respectively, in mean water depths somewhat greater than 3 m [*Hay and Mudge*, 2005]. The rotary sonars are Simrad Mesotech Model 971s operating at 2.25 MHz. Their performance characteristics in relation to bed form measurements in the nearshore zone have been described elsewhere [*Hay and Wilson*, 1994; *Ngusaru and Hay*, 2004; *Hay and Mudge*, 2005].

[9] The rotary sonar transducers were mounted at 71 cm and 76 cm mean heights above bottom at frame C and D, respectively. The transducer assembly is driven in azimuth in 0.225° increments. The data acquisition system was configured to acquire 5 complete (360°) images with 0.45° resolution in azimuth, and 0.9 cm resolution in range. The transmit pulse duration was 10 μ s. The backscatter signal was digitized (12 bit resolution) at 250 kHz and three-point block averaged. The units transmitted at each 0.225° step, and the backscatter profiles from two consecutive steps were averaged together. The block averaging in range and profile averaging in azimuth were implemented to reduce speckle noise in the individual 9.5 m diameter images. Each set of 5 images was acquired in about 3.7 min, at 10 min intervals during storm events and at 30 min intervals during the periods of relative calm between storms.

2.2. Sonar Image Processing

[10] The five images in each set were combined to produce a single composite image, as described by *Hay and Mudge* [2005]. This was done to reduce the effects of intermittent noise arising during SD97 mainly from (1) masking of the seabed returns by sediment suspension events and/or bubble clouds injected by breaking waves and (2) shadows cast on the seabed by fish swimming through the acoustic beam. The total number of composite fan beam images was 6820 at frame C, and 6774 at frame D. The range-azimuth backscatter profiles were slant range corrected and beam pattern compensated in range-azimuth space as outlined by *Hay and Mudge* [2005], and then interpolated to x - y Cartesian coordinates at 0.9×0.9 cm resolution.

[11] The composite images were used to create movies of bedstate evolution through time. These movies were reviewed and scour pit and other bedstate occurrences documented in a database. For each time interval in which scour pits were present, individual pits were captured as subimages. An edge detection algorithm was then applied to the subimages to obtain quantitative measurements of scour pit area and centroid location.

2.3. Forcing Statistics

[12] The velocity and pressure time series were partitioned into (1) the record means U , V , and P ; (2) the sea-and-swell band u_w , v_w , and p_w (0.05–0.3 Hz); and (3) the infragravity band u_{IG} , v_{IG} , and p_{IG} (<0.05 Hz). The sea-and-swell band and infragravity band constituents were obtained using forward and reverse passes of a fifth-order Butterworth digital filter. The rms wave orbital velocity in the sea-and-swell band is defined as

$$u_{\text{rms}} = \langle u_w^2 + v_w^2 \rangle^{1/2}, \quad (1)$$

and the significant wave orbital velocity is defined as $u_{1/3} = 2u_{\text{rms}}$ [*Thornton and Guza*, 1983]. The rms infragravity

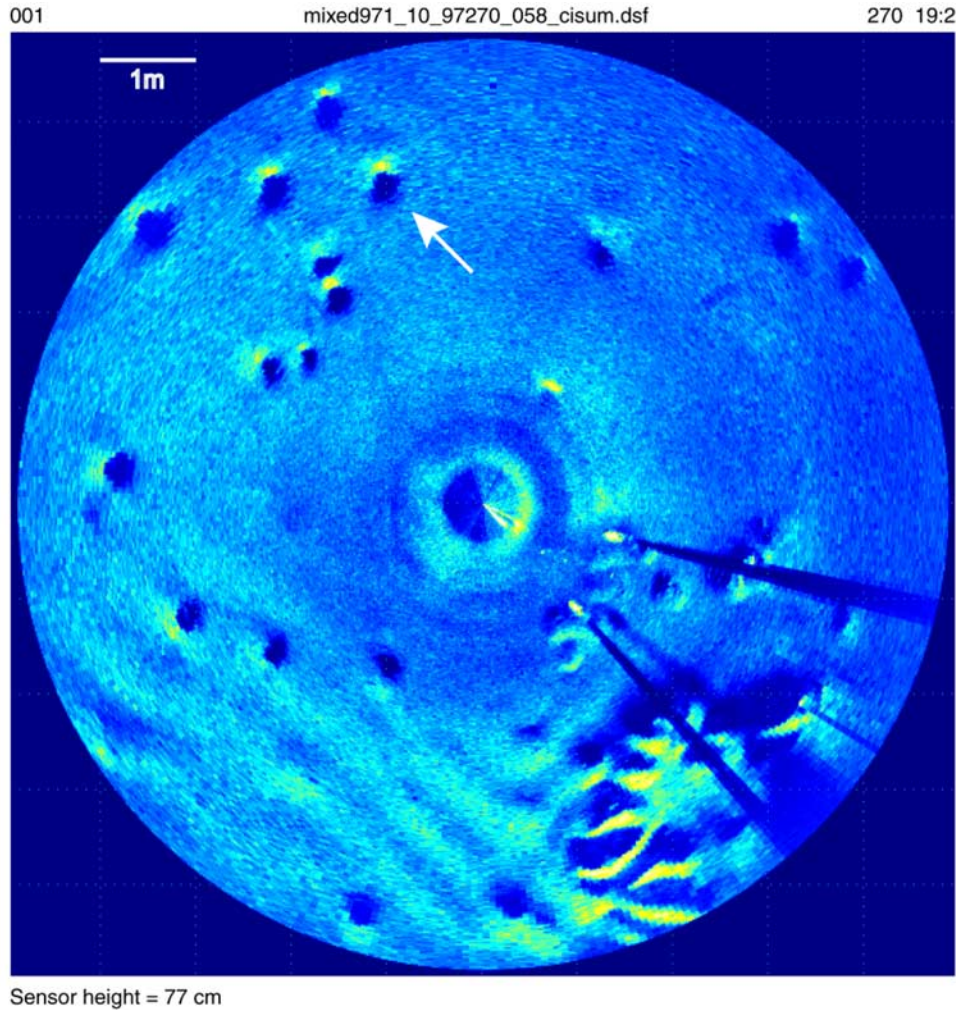


Figure 2. Representative rotary fan beam image of the seabed at frame C at 1920 LST on YD 270. Low-amplitude backscatter is blue; high-amplitude backscatter is yellow and white. The instrument frame is in the lower right quadrant: the bright echoes and radial acoustic shadows are caused by the frame legs. Offshore is toward the top. The grid indicates 1 m intervals. The arrow indicates a scour pit. There are more than 20 such features in this image, 20–50 cm in diameter and roughly circular.

wave velocity is defined similarly: $\mathcal{U}_{\text{rms}}^{\text{IG}} = \langle u_{\text{IG}}^2 + v_{\text{IG}}^2 \rangle^{1/2}$. The u components are positive shoreward, the v components positive toward the south (i.e., the directions of positive x and y).

[13] Skewness, Sk , and asymmetry, As , were computed for each data run from the sea-and-swell band velocity and pressure time series as follows:

$$Sk(x) = \langle x^3 \rangle / \langle x^2 \rangle^{3/2} \quad (2)$$

$$As(x) = Sk[\Im\{\mathcal{H}(x)\}], \quad (3)$$

where $\mathcal{H}(x)$ is the Hilbert transform of x , and \Im denotes the imaginary part. Note that this definition of asymmetry gives values identical in magnitude but opposite in sign to those reported by *Elgar et al.* [1990] (see also *Elgar* [1987]).

[14] Velocity and pressure spectra were estimated from the 1/2-hour-long records using Hanning-windowed, linearly detrended 200 point data segments with 50% overlap. The resulting spectra had 0.1 Hz resolution and 66 equivalent

degrees of freedom. The peak wave period, T_p , corresponds to the peak in the u spectrum.

[15] The grain roughness Shields parameter is given by [e.g., *Sleath*, 1984]

$$\theta_{2.5} = \frac{f'_w}{2} \frac{u_{1/3}^2}{g(s-1)d_{50}}, \quad (4)$$

where s is the sediment grain specific gravity (taken here to be 2.65, the value for quartz), g is the acceleration due to gravity, d_{50} is the median grain size, and f'_w is the fixed grain wave friction factor computed using Swart's formula with $2.5d_{50}$ for the physical roughness [*Nielsen*, 1992]. The grain size distributions at the two frames were very similar, with $d_{50} = 145 \mu\text{m}$ at frame C and $148 \mu\text{m}$ at D.

3. Results

[16] A representative image from frame C is shown in Figure 2. About 20 scour pits are present in the image, each

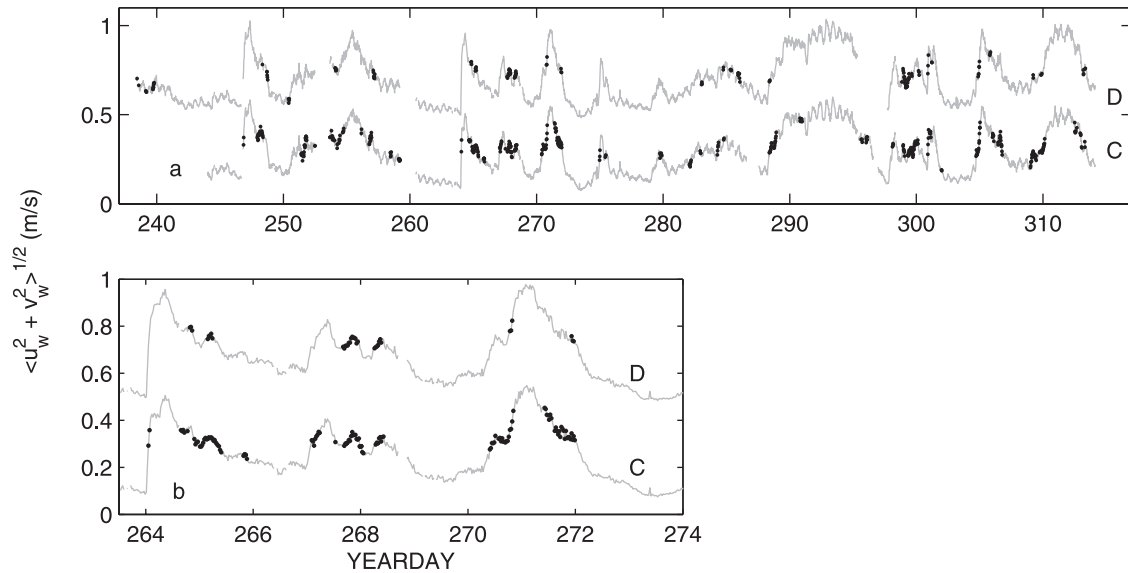


Figure 3. Time series of rms wave orbital velocity (shaded lines) and scour pit occurrences (dots) at frames C and D for (a) the full experiment and (b) a 10 day interval encompassing three storm events. The frame D data are offset by 0.4 m/s.

roughly circular with 20–50 cm diameters. Each pit is characterized by low-amplitude backscatter from the central region of the pit, due to the pit bottom and lower wall being within the acoustic shadow cast by the pit edge nearest the transducer. High-amplitude backscatter is generated from the pit’s far edge, where the upper pit wall faces the transducer. There are other features in this image: the long-crested meter-wavelength ripples at the lower left, and the short-crested shorter wavelength ripples immediately shoreward of the frame. These features will be discussed elsewhere.

3.1. Occurrence Versus Hydrodynamic Forcing

[17] Figure 3 shows the time series of rms wave orbital velocity at frames C and D, with the scour pit occurrences superposed. Fewer pits occurred at frame D than at C. At frame C, 53 scour pit episodes were identified between year day (YD) 237 and YD 313, resulting in a total of 2436 subimages of 485 different scour pits. (By “episode” we mean a period of time in which one or more scour pits was present in the sonar field of view.) Over the same period at frame D there were 21 scour pit episodes, yielding 345 subimages of 75 different scour pits. The u_{rms} peaks in Figure 3 demonstrate that up to 13 separate significant forcing events occurred over the full 77 day record. Scour pits formed during each of the 13 wave forcing events, and in all events scour pits appeared during both wave growth and wave decay.

[18] A striking feature of Figure 3 is the relatively narrow band of wave energies within which scour pits occurred. This sensitivity to wave energy is further illustrated by Figure 3b, which shows that at both frames the relatively small changes in local wave energy associated with semi-diurnal tidal modulations in water depth led to several scour pit episodes during the decay phase of two storm events. (Hence the number of scour pit episodes at frame C was greater than twice the number of storm events.) The relationship between wave energy and scour pit occurrence

is further reinforced by Table 1, which lists the experiment-mean values of hydrodynamic forcing parameters during all scour pit episodes at each frame. Of the parameters listed, the wave orbital velocity u_{rms} and the closely related grain roughness Shields parameter have standard deviations which are much smaller than their means. The other forcing parameters (longshore current speed, cross-shore mean current, wave orbital velocity skewness, wave orbital velocity asymmetry, incident wave angle) all have standard deviations which are comparable to or exceed their mean values, indicating that these parameters would not be good

Table 1. Experiment-Mean Hydrodynamic Forcing Parameters Versus Scour Pit and Lunate Megaripple Bedstates at Frames C and D^a

	Pits	Megaripples
	<i>Frame C</i>	
u_{rms} , m/s	0.33 ± 0.053	0.34 ± 0.058
T_p , s	8.2 ± 2.4	8.3 ± 2.4
$\theta_{2.5}$	0.70 ± 0.20	0.75 ± 0.23
$ V_b $, m/s	0.12 ± 0.15	0.22 ± 0.21
U , m/s	-0.081 ± 0.041	-0.071 ± 0.029
Sk_u	0.18 ± 0.24	0.19 ± 0.22
As_u	0.075 ± 0.054	0.059 ± 0.052
α , deg	0.46 ± 13.0	10.6 ± 15.0
$U_{\text{rms}}^{\text{IG}}$, m/s	0.060 ± 0.019	0.062 ± 0.020
	<i>Frame D</i>	
u_{rms} , m/s	0.31 ± 0.04	0.34 ± 0.049
T_p , s	7.9 ± 2.2	9.3 ± 3.2
$\theta_{2.5}$	0.65 ± 0.16	0.74 ± 0.19
$ V_b $, m/s	0.098 ± 0.12	0.16 ± 0.17
U , m/s	-0.086 ± 0.051	-0.062 ± 0.019
Sk_u	0.12 ± 0.21	0.25 ± 0.27
As_u	0.077 ± 0.055	0.045 ± 0.056
α , deg	0.40 ± 11.6	1.1 ± 14.4
$U_{\text{rms}}^{\text{IG}}$, m/s	0.054 ± 0.016	0.065 ± 0.024

^aThe values listed are the means over all instances of each bedstate $\pm\sigma$, the standard deviation (except the Shields parameter $\theta_{2.5}$ for which the \pm values are based on the σ for u_{rms}).

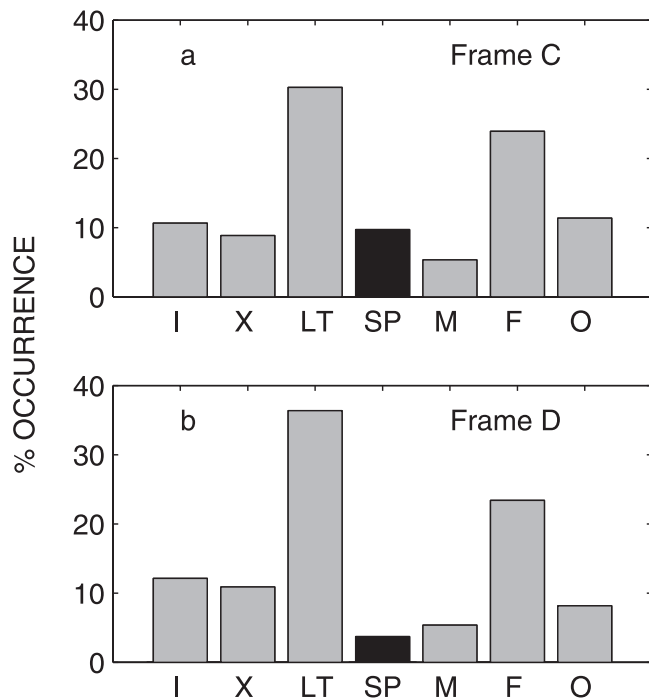


Figure 4. Percent occurrence of scour pits relative to other bedstates observed during SandyDuck97 at (a) frame C and (b) frame D. I, irregular ripples; X, cross ripples; LT, linear transition ripples; SP, scour pits; M, lunate megaripples; F, flat bed; O, other.

predictors of scour pit occurrence in the SD97 data. Infragravity wave velocities are an exception, with standard deviations which are 10–20% of the mean, like those for u_{rms} . However, the infragravity wave energies are small, 25 times smaller than the incident wave energies. Thus it is concluded that among these hydrodynamic forcing parameters, wave orbital velocity was the primary hydrodynamic factor affecting scour pit occurrence.

3.2. Occurrence Versus Other Bedstates

[19] The primary importance of u_{rms} in relation to scour pit occurrence is consistent with the findings of Hay and Mudge [2005] for principal bedstates during SD97. The term “principal” indicates the more frequent bedstates observed at frames C and D, i.e., irregular ripples, cross ripples, linear transition ripples and flat bed. Hay and Mudge [2005] have tabulated the experiment-mean values of the same forcing parameters as those listed in Table 1 for each principal bedstate. Included in Table 1 are their data for the lunate megaripple state, from which it can be seen that the range of u_{rms} values corresponding to scour pit occurrence overlaps the lunate megaripple range. Since some scour pits evolved into lunate megaripples, this overlap is expected.

[20] Of the scour pits which formed during the growth phase of wave-forcing events, some occurred after irregular or linear ripples, forming on the ripple slope near the crest or along the troughs of long-wavelength linear ripples (e.g., Figure 2). Some occurred simultaneously with cross ripples, or with linear ripples like those in Figure 2, or with linear transition ripples or lunate megaripples. Many, however,

occurred on an otherwise featureless flat bed, especially following flat bed conditions during wave decay (for example, at frame C on YD 271 during the decay phase of the YD 270–272 event). Thus scour pit formation does not appear to require bed roughness associated with pre-existing bed forms.

[21] The percentage occurrences of the different bedstates in the fan beam imagery from frames C and D are presented in Figure 4. These percentages are based on the number of images in which a given bedstate occurred, relative to the total number of images acquired (6820 at frame C, and 6774 at frame D). In computing the percentages, images acquired at 10 min intervals were given a weight of unity, and those at 30 min intervals a weight of 3, thereby removing the occurrence frequency bias arising from the use of 10 min acquisition intervals during energetic conditions and 30 min intervals during quiescent conditions. As Figure 4 indicates, scour pits occurred as frequently as many of the “principal” bedstates. At frame C, scour pits occurred more frequently than lunate megaripples. By this measure, therefore, scour pits could justifiably be added to the list of principal bedstates observed in the outer surf zone during this experiment.

3.3. Diameter and Depth

[22] The probability distribution function (pdf) of scour pit diameters is shown in Figure 5. In this figure, and in the remainder of the paper unless otherwise indicated, “pit diameter” corresponds to the diameter of the circle equal in area to the central acoustic shadow region, i.e., the dark blue areas in Figure 2. The distributions for both frames are broadly similar. Both distributions peak at about 20 cm diameter, and tail off quickly to low probabilities at diameters greater than 50 cm. Note that the large-diameter values include the lunate megaripples which developed within the sonar field of view from initial pits, as there was no obvious objective criterion for identifying the point at which a growing pit became a lunate megaripple.

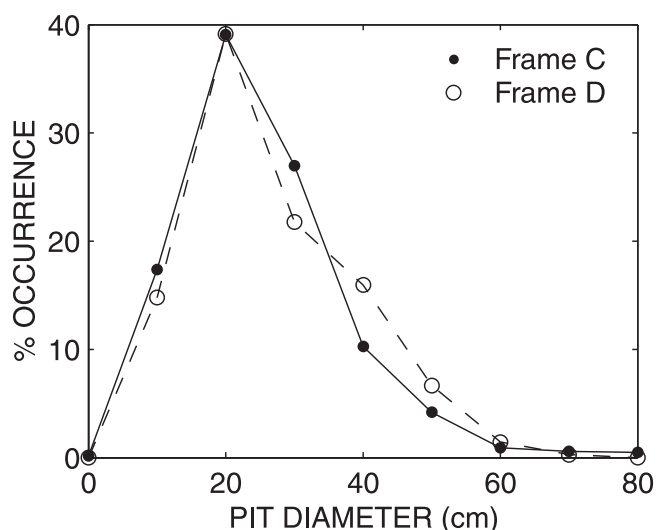


Figure 5. Distribution of scour pit diameters. Values are from the fan beam imagery and are likely 15–20% smaller than actual diameters (see equation (6) and related discussion).

Table 2. Summary of Scour Pit Characteristics^a

	N	\overline{D} , cm	D'_{50} , cm	N	\overline{T} , hours	T_{50} , hours
<i>Frame C</i>						
All	2436	25.2	23.1	485	0.90	0.50
Wave growth	243	33 ± 12	31	243	1.0 ± 1.7	0.58
Wave decay	192	28 ± 10	27	192	0.81 ± 1.2	0.42
<i>Frame D</i>						
All	345	26.5	23.5	75	0.73	0.50
Wave growth	36	28 ± 9	31	36	0.53 ± 0.5	
Wave decay	25	32 ± 8	27	25	0.97 ± 1.4	

^aAbbreviations are as follows: N , number of scour pits; \overline{D} , D'_{50} , mean and median observed pit diameter over the lifetime of each scour pit, respectively; \overline{T} , T_{50} , mean and median lifetime, respectively. Numbers following ± represent standard deviations. See text for explanation of the different N s.

Including the megaripples certainly contributes to the skewing of the distribution toward large values. Summary statistics for the distributions in Figure 5 are listed in Table 2, in the rows labelled “All,” indicating all subimages.

[23] Also listed in Table 2 are values of mean and median pit diameter for the wave growth and decay phases. In this case, the means and medians are based on the distribution of average diameter for each pit, and the standard deviations listed represent the variation about the specified value among the number N of individual pits indicated. There is little difference in the mean and median diameters during storm growth and decay at either frame.

[24] The depth of scour can be determined indirectly from the fan beam imagery if the pit wall is assumed to be close to the angle of repose. A means of testing this assumption is provided by the rotary pencil beam images, from which a bed elevation profile along a single cross-shore line is determined [Ngusuru and Hay, 2004; Hay and Mudge, 2005]. In a small number of instances, a scour pit was more or less centered on this line, providing an elevation profile across the pit. As an example, Figure 6 shows three consecutive profiles, 10 min apart, through the same scour pit. The apparent depth is not more than 3 cm. However, the pit was 3 m distant from the sonar which was 80 cm high, so the base of the pit was likely obscured by the acoustic shadow cast by the near edge of the pit, as demonstrated next.

[25] Letting h_s be the depth of scour, h'_s the apparent depth, ϕ the incident grazing angle (the elevation angle of the line of sight between the transducer and the edge of the pit nearest the transducer), and β the slope of the pit wall, then

$$h'_s/h_s = 2 \tan \phi / (\tan \beta + \tan \phi). \quad (5)$$

For $\phi = 15^\circ$ and $\beta = 23^\circ$ or 33° , which are respectively the residual angle of shearing and the angle of initial yield [Sleath, 1984], the pencil beam profiles would according to equation (5) underestimate the scour pit depths by 23–42%. Thus the actual depth of scour indicated by the profiles in Figure 6 would be 4–5 cm. For comparison, the median pit diameter from the fan beam images (≈ 25 cm, Table 2) and the above values of β give scour depths of 5–9 cm, which are within a factor of 2 or less of the range of values obtained from the pencil beam profiles using

equation (5). Since it is not certain that the pencil beam sliced through the center of the pit, this level of agreement is satisfactory and we conclude that the depths of scour are $O(10)$ cm.

[26] The pit diameter from the fan beam images, as obtained from our edge detection technique, is likely less than the actual diameter. Comparing Figure 6 with Figure 2, it can be seen that the bright echo from the steep slope facing the transducer would reduce the diameter of the acoustic shadow zone in the radial direction. The same geometric analysis upon which equation (5) is based yields

$$\hat{D}/D = \tan \beta / (\tan \beta + \tan \phi) \quad (6)$$

for the ratio of apparent diameter in the radial direction, \hat{D} , to the actual pit diameter, D . The above values of ϕ and β give \hat{D} values which are 30–40% less than the likely actual diameters. If the pit shadow area is assumed to be elliptical, with minor axis \hat{D} and major axis D , then the observed equal area diameter is $D' = \sqrt{\hat{D}D}$. Thus the equal area

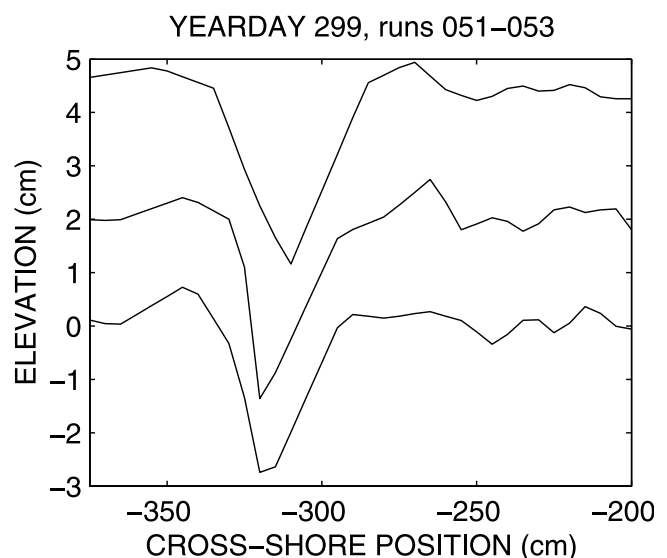


Figure 6. Bed elevation profiles through a scour pit. The profiles were taken 10 min apart, starting at 0757 LST on YD 299. Successive profiles have been offset in the vertical by +2 cm.

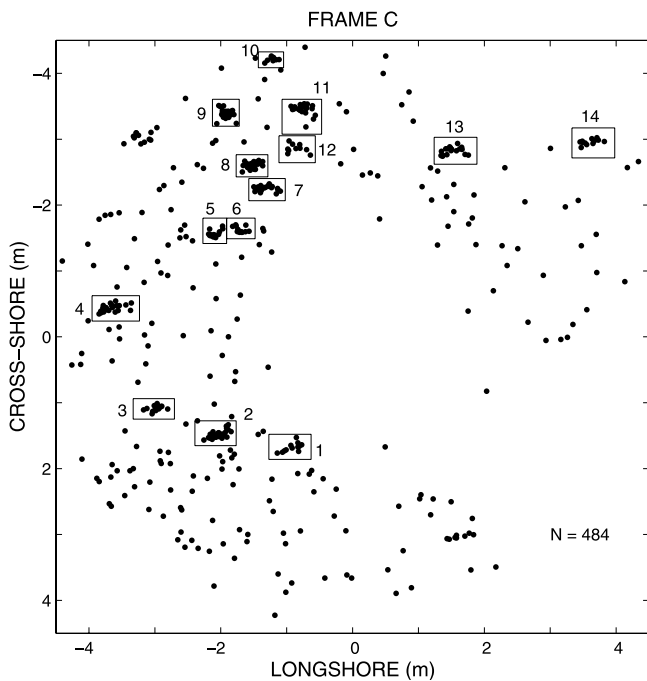


Figure 7. Initial locations of scour pits at frame C. Numbered boxes indicate pit clusters. (See also Figure 9.)

diameters estimated here are expected to be only 15–20% less than D .

3.4. Spatial Distribution

[27] The locations at which a given scour pit first appeared within the sonar field of view are shown in Figure 7 for frame C and in Figure 8 for frame D. Excluding the lower right quadrant occupied by the

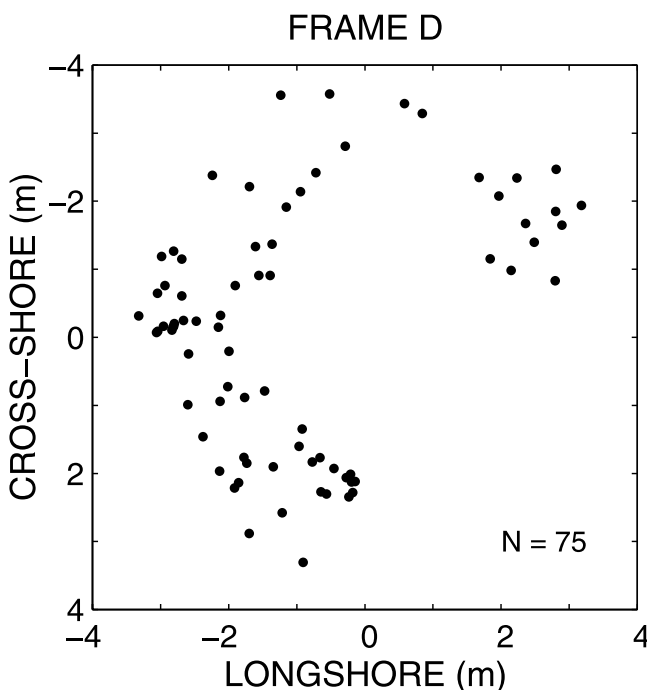


Figure 8. Initial locations of scour pits at frame D.

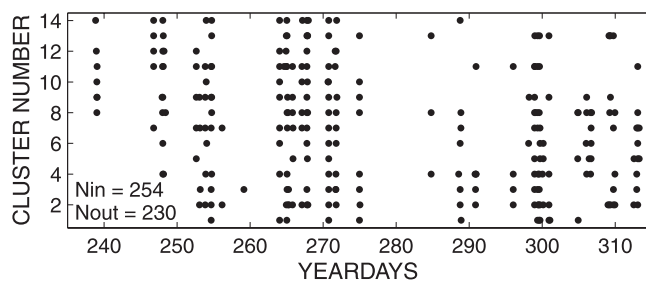


Figure 9. Time sequences of scour pit first occurrences in the clusters at frame C indicated in Figure 7. More than 50% (254 of the 484 total) of the pits were in these 14 clusters, which, as the time sequences indicate, in most instances persisted (or reemerged) throughout most of the experiment.

instrument frame, the distribution of first occurrences is essentially isotropic (independent of azimuth) for both frames. These figures also indicate that pits were seldom detected within an approximately 1 m radius circle centered at the transducer location. As can be seen from Figure 2, this inner zone of apparent pit nonoccurrence is due in part to the seabed within a ≈ 0.5 m radius not being imaged (because of the transducer height and beam pattern). In addition, the pits would not be as readily identifiable in the images at steep grazing angles, and thus not at short ranges, because of their low relief.

[28] Thus Figures 7 and 8 indicate that within the ≈ 50 m² annulus lying between radii of 1 m and 4.5 m, and occupying somewhat more than three quadrants, the spatial distributions of scour pit first occurrences were essentially isotropic. At frame C when scour pits were present, there were as few as 1 and as many as 30 individual pits within this area at any one time. The mean areal number density was 0.09 m⁻². At frame D, there were as few as 1 and as many as 12 individual scour pits present, with a mean number density of 0.07 m⁻².

[29] Pit spatial distribution was not homogeneous, however. At frame C, there was a definite tendency for scour pits to occur at nearly the same location during different storm events. Fourteen of these repeat appearance regions are indicated by the numbered boxes in Figure 7. Of the 485 pit locations observed at frame C, more than 50% (254) occurred within these 14 clusters. For each cluster, Figure 9 shows the times of scour pit first occurrence, demonstrating that scour pits reoccurred within the cluster areas throughout the experiment. (Similar clustering is indicated in the frame D data, near 0 m cross-shore and 2 m longshore in Figure 8 for example, but is less distinct: an effect likely due at least in part to the smaller number of pit occurrences at this frame.)

[30] Could the reoccurrence of pits in roughly the same locations 50% of the time be merely the result of chance? To examine this question, we first model the distribution of pits scattered at random within a 50 m² grid, divided into square cells 50 cm on a side. The probability of pit occurrence is assumed to be uniformly distributed over the x and y intervals set by the outer dimensions of the grid (10 and 5 m respectively). The grid was populated with 500 non-overlapping virtual pits, each 10 cm in diameter. The grid area is comparable to the area of the 270° annulus excluding the instrument frame, and similarly the cell size is compa-

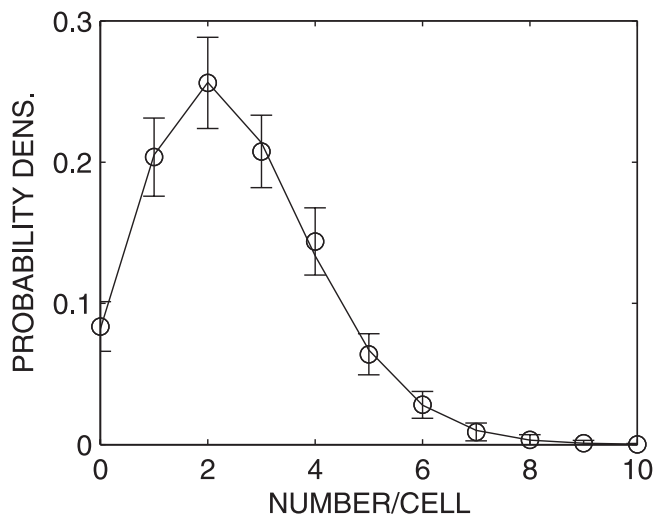


Figure 10. Simulated probability distribution of scour pit initial locations. Points with ± 1 standard deviation error bars are the model results. The solid line is the Poisson distribution, equation (7), with the mean probability density of the simulations, i.e., $\lambda = 2.5$.

table to the sizes of the boxes enclosing the pit occurrence clusters in Figure 7. The diameter and total number of the virtual pits are also comparable to the diameters and total number of the scour pits at frame C. The resulting probability distribution of occurrences per cell is presented in Figure 10. The plotted points and error bars indicate the means and standard deviations obtained from 50 independent realizations. The solid line corresponds to a Poisson distribution [Feller, 1968]

$$p(n) = \frac{1}{n!} (\lambda\tau)^n \exp(-\lambda\tau), \quad (7)$$

where $p(n)$ is the probability density for n occurrences per cell, τ is the effective cell width (i.e., interval size), and λ is the mean probability density. We define λ to be the mean number per cell, and thus $\tau = 1$. The solid line in Figure 10 corresponds to equation (7) with λ equal to the overall mean number per cell of the simulated distributions. The results in this figure demonstrate that, were the pit locations to have been distributed at random with uniform probability throughout the designated detection area, the occurrences per cell would be Poisson distributed.

[31] Figure 11 shows the observed distribution of pit locations at frame C. This distribution was obtained by subdividing the 4.75 m \times 4.75 m field encompassing the sonar image into cells 50 cm square, and excluding those cells with centers located within the lower right quadrant occupied by the instrument frame, and also those with centers at radii greater than 5 m or less than 1.3 m, i.e., the areas outside the detection region (Figure 7). The solid line is the predicted distribution from equation (7). Unlike the simulated pit locations, the data are not Poisson distributed: the observed probability of zero occurrence is much higher than predicted, and the predicted probability of large numbers of occurrences per cell falls to zero much sooner than the observations indicate.

[32] The inset in Figure 11 shows the distribution of observed pit locations after replacing each of the 14 clusters by a single point corresponding to the mean of all locations within the cluster. The distribution of the pit locations so modified is much better represented by a Poisson distribution: the observed and predicted probability densities at zero occurrence are quite similar, and the occurrence probability densities fall to zero at similar rates with increasing n . Some differences remain: the observed probabilities for $n = 0$ and $3 \leq n \leq 5$ are still somewhat higher than Poisson. It seems likely that these differences are due to residual clustering within the data: for example, the probable cluster near $x = -3$ m, $y = -3$ m in Figure 7.

3.5. Lifetimes and Growth Rates

[33] The lifetimes of individual scour pits were sometimes shorter than the 10 min interval between runs or, for those that developed into lunate megaripples, as long as 9.2 h. The distributions of pit lifetimes at frames C and D are shown in Figure 12, and are very similar. The mean and median lifetimes for the distributions in this figure are listed in Table 2, in the rows labelled "All," in this case indicating all scour pits. The mean and median lifetimes are also very similar for the two frames, being about 1 and 0.5 h respectively.

[34] Examples of pit diameter growth and decay curves are shown in Figure 13. Within the scatter of the observations, the curves are linear. The r^2 values for the best-fit

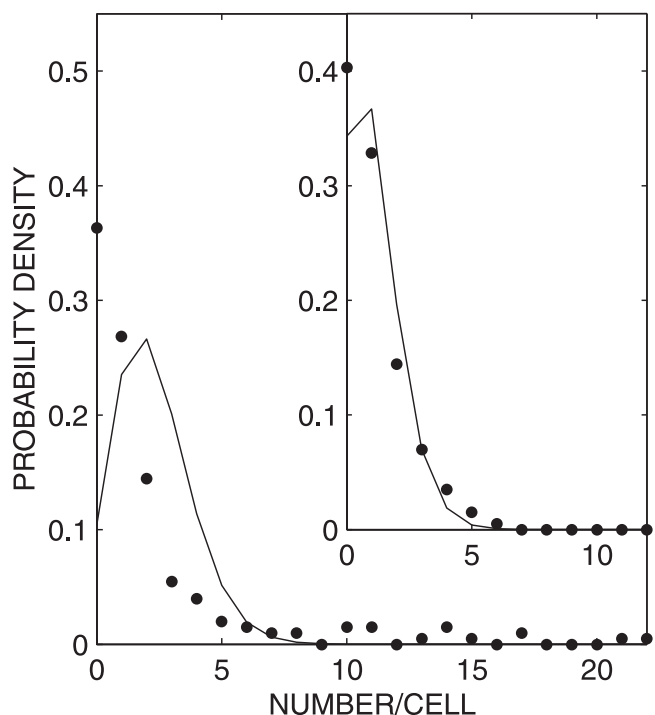


Figure 11. Observed probability distribution of initial locations of scour pits at frame C ($N = 455$; occurrences in the lower right quadrant occupied by the frame are excluded). The solid line is the Poisson distribution with the same mean probability density ($\lambda = 2.26$). The inset shows the observed and Poisson distributions with the pit location clusters replaced by a single location ($N = 215$), with mean density $\lambda = 1.07$.

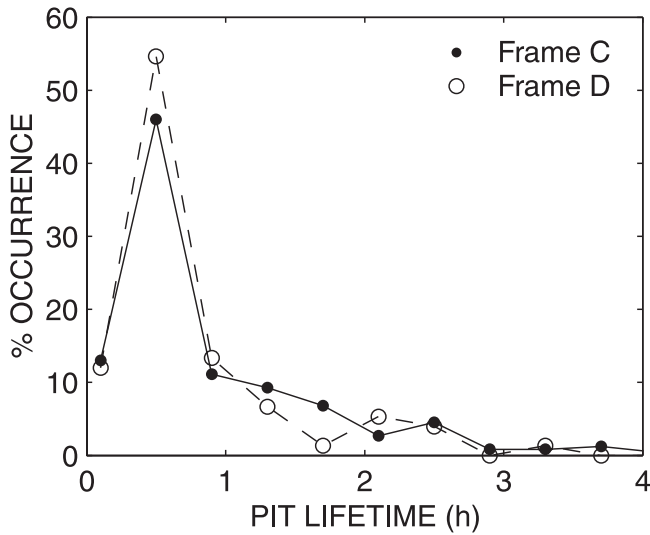


Figure 12. Lifetimes of individual scour pits.

straight lines to the observed points are quite high (>0.9) in these two cases. The distributions of pit diameter rates of change determined in this manner with r^2 values greater than 0.7 are shown in Figure 14, for both storm wave

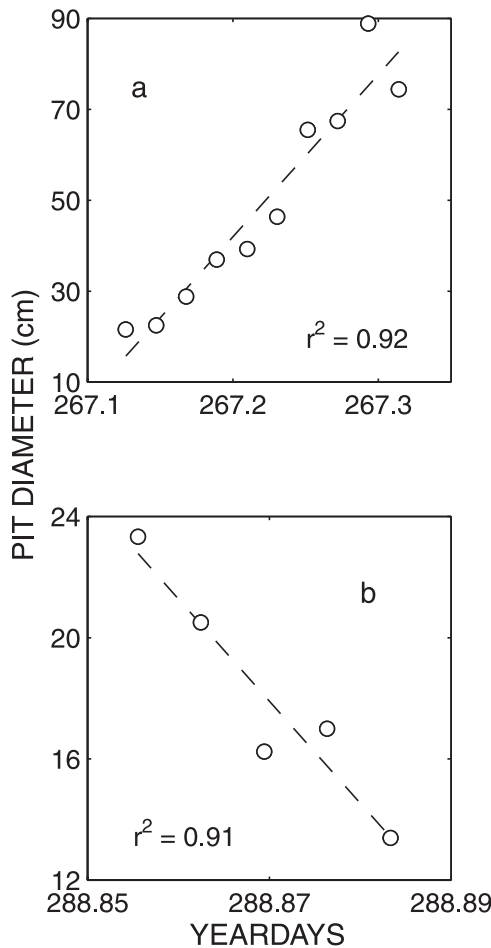


Figure 13. Examples of (a) growth and (b) decay of individual scour pits.

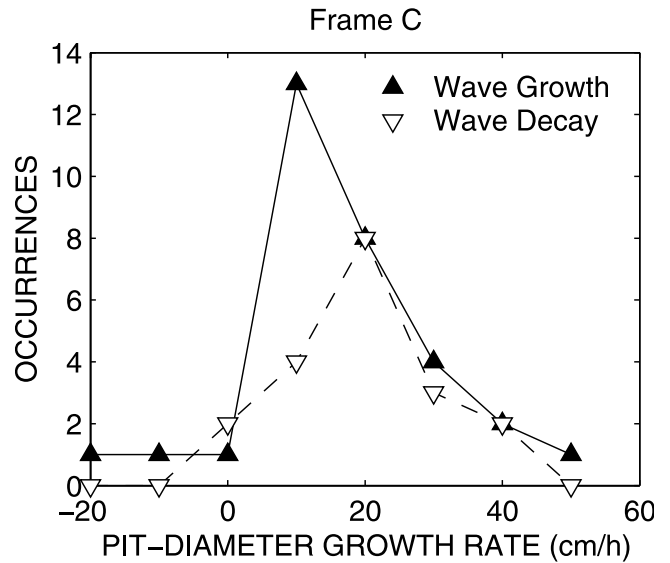


Figure 14. Distributions of pit diameter growth rates, based on linear fits as in Figure 13, with $r^2 > 0.7$.

growth and decay, at frame C. The distributions are skewed toward positive values (overall, 91% of frame C scour pits were growing), with 10 cm/h being a typical value.

[35] Also listed in Table 2 are values of mean and median pit lifetimes for the wave growth and decay phases. The standard deviations are large, too large to indicate a significant difference in typical pit lifetime either between frames or between storm growth and decay. (Note that median values are not listed for frame D due to the small sample size.)

3.6. Nuclei

[36] Scour at the base of cylindrical piles in waves and currents has been studied extensively [*Sumer and Fredsoe, 2002*], and Figure 15a shows an example of a scour pit surrounding one of the frame legs. During the SD97 experiment, from YD 279 to YD 286, hydrozoans formed 5- to 10-cm-thick sand-encrusted colonies on the instrument frames and support pipes. This material, which had the consistency of a very friable and porous sandstone, was removed from the frames by divers on YD 286, leaving various-sized chunks on the seabed. Figure 15b is a subimage showing one of these fragments roughly 10 cm in diameter at the center of the distinct scour pit which had formed around it. Thus one candidate mechanism for the formation of the pits described here is scour about an object of some kind on the sea bed: e.g., about a “nucleus.” To be unambiguously detectable in the sonar imagery, such nuclei would have to be at least 1 cm (1 range bin) in diameter, and very likely larger (as in Figure 15b), and would have to protrude above the acoustic shadow zone in the central region of the pit.

[37] To investigate this possibility, the pit subimages were examined for the presence of nuclei. An example of a pit with a nucleus is shown in Figure 15c. However, nuclei were discernable in only 10–20% of the subimages. At frame C, nuclei were found in the subimages for 32 of the 485 different pits, about 7%. At frame D, 15 pits contained nuclei, or 20% of the 75 different pits identified at this frame. Of those pits with nuclei, the nucleus typically was

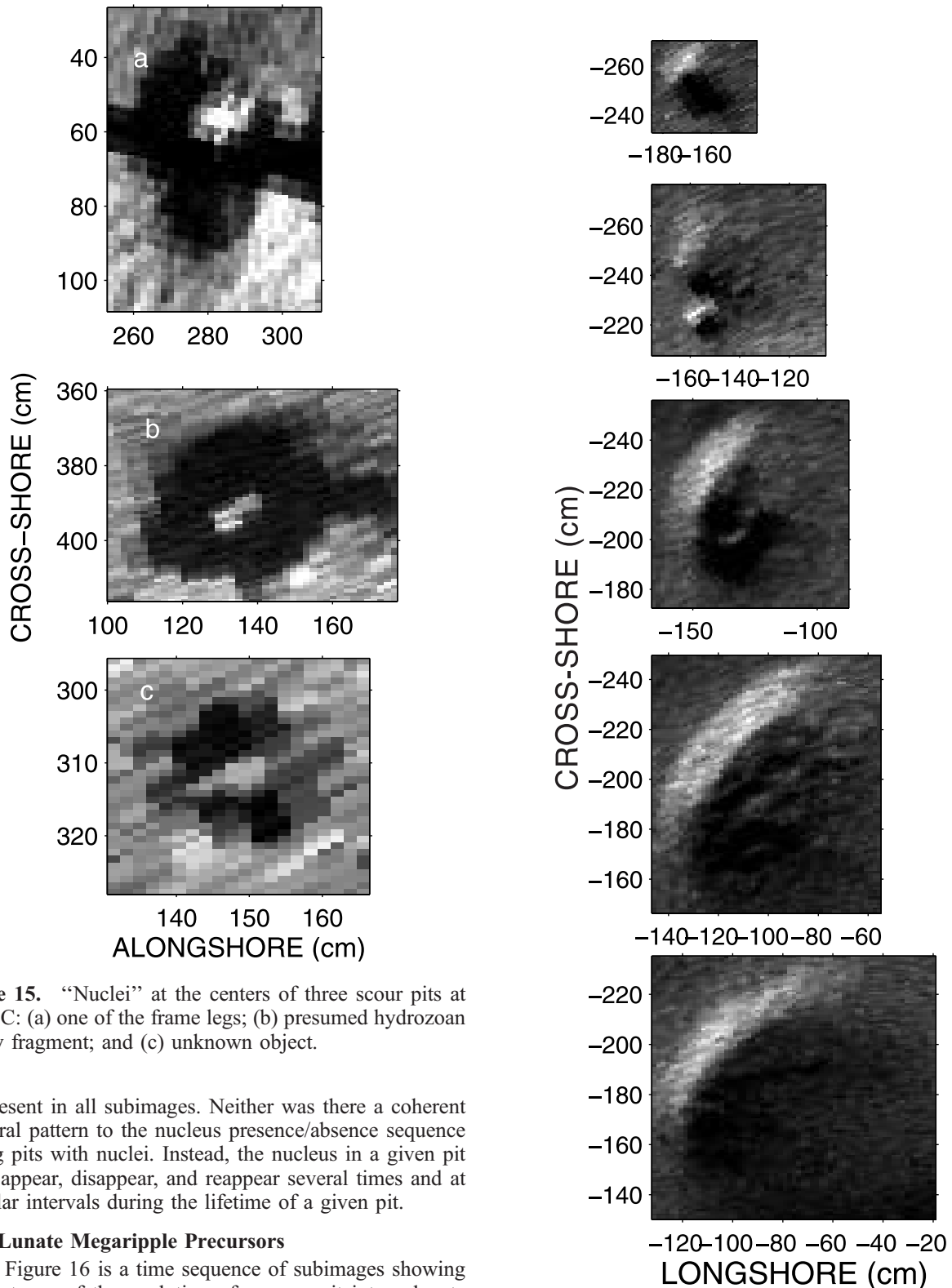


Figure 15. “Nuclei” at the centers of three scour pits at frame C: (a) one of the frame legs; (b) presumed hydrozoan colony fragment; and (c) unknown object.

not present in all subimages. Neither was there a coherent temporal pattern to the nucleus presence/absence sequence among pits with nuclei. Instead, the nucleus in a given pit could appear, disappear, and reappear several times and at irregular intervals during the lifetime of a given pit.

3.7. Lunate Megaripple Precursors

[38] Figure 16 is a time sequence of subimages showing one instance of the evolution of a scour pit into a lunate megaripple. The increase in scale and the progressive development of the crescentic shape characteristic of lunate megaripples in rotary sonar imagery [Ngusaru and Hay, 2004; Hay and Mudge, 2005] are evident in the sequence. The megaripple in Figure 16 was migrating onshore and toward the south, the direction faced by the concave side of the high backscatter amplitude crescent. There were a total of 13 instances in which scour pits away from the instru-

Figure 16. Subimage sequence showing development of a lunate megaripple from a scour pit on YD 267. From top to bottom, times are 0332, 0402, 0502, 0632, and 0702 LST. During this 3.5 hour time segment the megaripple migrated 0.5 m shoreward and 1.5 m alongshore in the southward direction.

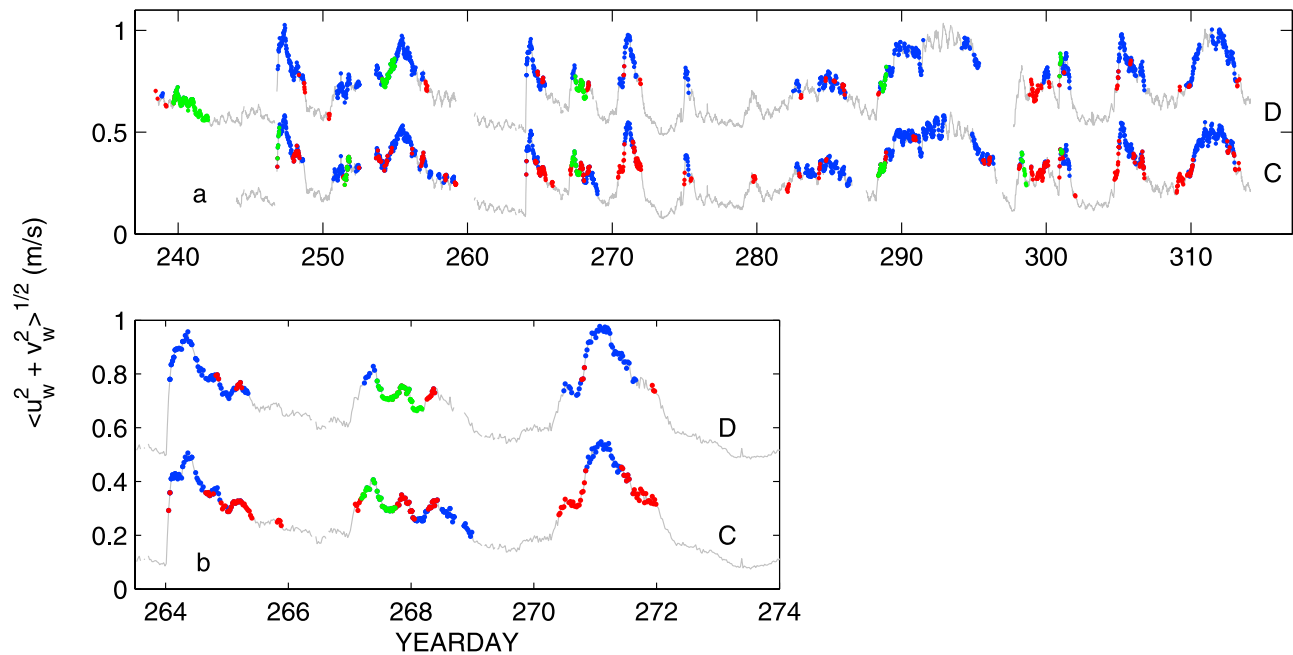


Figure 17. Time series of rms wave orbital velocity and scour pit occurrences at frames C and D shown in Figure 3, but with occurrences of lunate megaripples (green dots) and flat bed (blue dots) added. Red dots indicate scour pits. (a) Full data set. (b) Expanded view of three forcing events. The semidiurnal variations in u_{rms} are due to water depth changes associated with the semidiurnal tide. The frame D data are offset by 0.4 m/s.

ment frame developed into lunate megaripples: 12 at frame C, 2 of which were from scour pits around probable hydrozoan colony fragments, and 1 at frame D.

[39] The similarity between the experiment-mean hydrodynamic conditions for scour pit and lunate megaripple occurrence, and the importance of wave orbital velocity compared to the other hydrodynamic forcing parameters, have already been discussed (see Table 1). Figure 17 presents the time series of u_{rms} and scour pit occurrence, with the flat bed and megaripple occurrences superimposed. Note the previously mentioned point that the scour pits occurred both before and after flat bed. The comparatively low occurrence frequency of lunate megaripples is again evident. Also evident is the fact that, in these time series, lunate megaripples need not be preceded by scour pits. There are two explanations: (1) lunate megaripples do not form from these scour pits only; (2) lunate megaripples sometimes formed elsewhere and subsequently migrated into the sonar field of view.

[40] In 4 of the 6 lunate megaripple episodes at frame C and 3 of the 5 episodes at frame D, megaripples were generated at frame legs. Leg-generated megaripples therefore provide the first of the two explanations for megaripples sometimes occurring in Figure 17 without scour pit precursors. Leg-generated megaripples also provide unambiguous evidence for flow disturbance by obstacles at the sediment-water interface being a mechanism for lunate megaripple genesis.

[41] At each of frames C and D, one megaripple episode was due solely to a single large megaripple migrating into the field of view. During the other episodes, in addition to the locally generated lunate forms, there were several instances of fully developed megaripples migrating into

view at both frames. Thus megaripples generated nonlocally represent the evidence for the second of the two explanations above for megaripple occurrence in the absence of a scour pit precursor. Importantly, these intruding megaripples also demonstrate that lunate megaripples formed at large distances from the instrument frames: that is, at distances exceeding 5 m.

3.8. Cross-Shore Distribution

[42] Scour pits were also observed closer to shore at another frame (F). As shown in Figure 1, frame F was located at the same distance offshore as frame A but 110 m farther south. No pits were observed at frame B because it did not have a fan beam sonar.

[43] The data return from the two inner frames, A and F, was very limited. Because the inner bar did not migrate offshore in the autumn as expected, the water depth at these frames was very shallow throughout the experiment and the instruments were buried much of the time as a result. Useful seabed images were nevertheless acquired at both locations, though for limited periods of time. The return from frame F was somewhat greater, per unit time deployed, because it was jacked up on its pipe legs by SCUBA divers after being deployed. While no scour pits were observed at frame A, a total of 10 occurred at frame F on YDs 259, 284, 287 and 288. None developed into lunate forms. Nevertheless, these results demonstrate that scour pits did occur in the inner surf zone during SD97.

[44] Finally, the evidence for higher occurrence rates at frame C compared to D is definitive. This result holds not only for total numbers over the full length of the record, but also for individual storm events, and typically also for the wave growth and decay phases for each of

these events. The difference is noteworthy in part because it exists despite the highly similar wave orbital velocity statistics, mean longshore current speeds, mean cross-shore current velocities, and grain size distributions at the two locations. Does the difference indicate a real cross-shore trend, perhaps associated with a shoreward increase in spatial density of pit nuclei? Or could the difference be due simply to patchiness in the spatial distribution of such nuclei?

4. Discussion

4.1. Comparisons With Other Studies

[45] In a nearshore field study using time lapse underwater video, Palmer [1969] found that the diameters of scour pits formed around 5–20 cm diameter rocks on sandy substrates were about 4 times the rock diameter. Thus Palmer's pit diameters for rock obstacles were in the 20–80 cm range, which is comparable to the pit diameters reported here. Palmer's range of rock diameters was also comparable to the 10 cm diameter hydrozoan colony fragment in Figure 15b, and to the 5 cm diameter of the unknown object in Figure 15c.

[46] The recent book by Sumer and Fredsoe [2002] provides a comprehensive summary of seabed scour around coastal engineering structures. Quantitative knowledge of scour is based primarily on laboratory experiments, with the single vertical pile being the obstruction type among those extensively studied which is most relevant here. The ratio of scour depth at equilibrium, S_∞ , to vertical pile diameter, d_{vp} , is given by their equation (3.20):

$$S_\infty/d_{vp} = 1.3[1 - \exp(-0.03(KC - 6))], \quad (KC \geq 6). \quad (8)$$

KC is the Keulegan-Carpenter number, given by

$$KC = u_m T_p / d_{vp}, \quad (9)$$

where u_m is the wave orbital velocity amplitude above the wave boundary layer, and T_p is the wave period. Equation (8) was based initially on experiments with regular waves, but Sumer and Fredsoe [2001] have shown that the same relation also applies to scour in irregular waves, provided $u_m = \sqrt{2}u_{rms}$. The numbers in Table 1 give $KC \approx 370/d_{vp}$ (d_{vp} in cm). Equating the 5–20 cm obstacle diameters above with d_{vp} , we obtain $75 \geq KC \geq 18$ and equation (8) gives $S_\infty = 6$ –8 cm. These scour depths are comparable to the $O(10)$ cm values estimated from the sonar imagery.

[47] Scour due to combined waves and currents acting on a vertical pile has been investigated by Sumer and Fredsoe [2001]. The parameter

$$U_{cw} = U_c / (U_c + u_m), \quad (10)$$

where U_c is the near-bed current speed, is their measure of the relative magnitudes of the mean current and the wave orbital velocity. Again taking $u_m = \sqrt{2}u_{rms}$, and $U_c = |V|$, the values in Table 1 give 0.2 as the experiment-mean value of U_{cw} for all scour pit episodes at frame C, with a range of 0–0.4 (based on the standard deviation of $|V|$). Noting that since Sumer and Fredsoe [2001] used U_c at a height of $d/2$ whereas our measurements of V were made farther from the bed at 35 cm nominal height, the above values of U_{cw} are

likely overestimates. Thus Sumer and Fredsoe [2001, Figures 4 and 5] indicate that the depths of scour for the conditions here would be expected to be similar to those for waves alone, as given by equation (8).

[48] Laboratory studies indicate that scour growth decreases exponentially with time [Sumer and Fredsoe, 2002; Voropayev et al., 2003]; that is,

$$S(t) = S_\infty[1 - \exp(-t/\gamma T)]. \quad (11)$$

Voropayev et al. [2003] investigated the timescale of scour for single short cylinders lying horizontally on a sand substrate subjected to nonlinear progressive waves. They obtained a value of 525 for γ , indicating an e-folding time of about 500 wave periods and, similar to the result of Herbich et al. [1984]), a timescale of about 1000 wave periods to reach equilibrium depth (S_∞). On this basis and our 6–10 s wave period range (Table 1), e-folding times of 0.9–1.2 hours would be expected for the SD97 pits. These times are comparable to but larger than the range of mean and median scour pit lifetimes listed in Table 2, indicating that equilibrium scour depths would seldom have been reached.

[49] For times such that $t \ll \gamma T$, pit growth rate is given by $dS/dt \approx S_\infty/\gamma T$. Setting S_∞ equal to the values obtained above, and again using wave periods of 6–10 s, the expected range of initial deepening rates would be 5–9 cm/h. Pit diameter grows at the rate $(dS/dt)/\tan \beta$. With β equal to 30°, the predicted range of diameter growth rates is then 9–15 cm/h, comparable to the 10–20 cm/h peaks in the observed growth rate distributions (Figure 12).

[50] Briefly summarizing, the comparisons to laboratory studies through equations (8)–(11) indicate that the geometry and growth rates of the SD97 scour pits are roughly comparable to those produced by thin vertical piles, and that the effects of the mean current on scour properties are expected to have been small relative to those of the waves. There are questions certainly, including in particular the unknown effects of irregular waves on the value of γ . Also, it must be pointed out with respect to γ that Sumer and Fredsoe [2002] argue that it is not a constant but a function of both KC and the Shields parameter. Their results are for Shields parameters below 0.2 which is much lower than the 0.6–0.7 range appropriate here (Table 1), and so are not directly applicable. The trend indicated by their results, however, is toward shorter e-folding times with increasing Shields parameter, which could offset the longer response times expected in irregular waves. The comparison to Palmer's field study indicates that our scour pit diameters are similar to his observations for scour around rock obstacles, and helps to place reasonable limits on the size of possible obstacles. Furthermore, Palmer's observation [see also Voropayev et al., 2003] that the scour process can lead to an object sinking within its scour pit below the level of the surrounding seabed, where it would be concealed by the acoustic shadow from the pit lip, could help to explain the absence of nuclei in the majority of the subimages.

4.2. Possible Origins and Candidate Obstacles

[51] The above comparisons indicate that a likely origin for the SD97 pit features is scour about naturally occurring obstacles on or embedded within the seafloor. In addition,

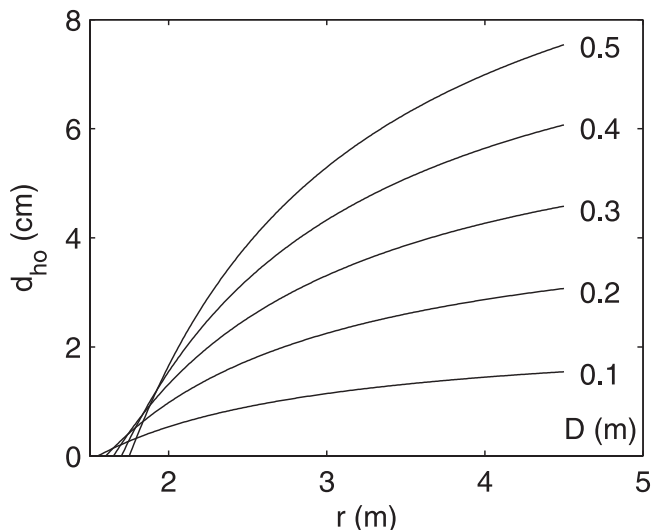


Figure 18. Hidden obstacle diameter, d_{ho} , as a function of radial distance, r , for different pit diameters, D . See equation (12).

50% of the pits were nonrandomly distributed within the detection area, reoccurring instead at nearly the same locations from storm event to storm event. This occurrence clustering suggests the presence of something within each cluster area which causes the scour, and therefore also supports the obstacle hypothesis. Recall as well that scour pits form on an otherwise flat bed during storm decay, and therefore appear not to require a precursor bed form. Finally, the specific instance of pits forming around hydrozoan colony fragments left on the seafloor after being scraped off the frame is direct evidence of scour pits forming around a compact obstacle.

[52] What might the obstacles be? There are a number of candidates: (1) stones and pebbles; (2) large shells or shell fragments; and (3) burrows formed by living organisms. *Schwartz et al.* [1997] reported finding gravel zones and isolated granules and pebbles in vibrocores from the study area in ≈ 3 m water depths. Pebble diameters were not reported. (The granule and pebble size ranges according to the Udden-Wentworth scale are 0.2–0.4 cm, and 0.4–6.4 cm, respectively.) Large numbers of conch shells were found washed up on the shoreface after one of the SD97 storm events. The dimensions of these shells were typically about 20 cm long by 10 cm largest outside diameter. *Hill and Hunter* [1976] have reported finding chimney structures formed by burrowing ghost shrimp in the bar-trough system in the inner surf zone of a beach on the Gulf of Mexico coastline, and show a photograph of scour pits around these chimneys (their Figure 19b). The ghost shrimp chimneys were 6–7 mm in diameter. For the experiment-mean conditions in Table 1, the corresponding values of KC would range from about 600–500, and of S_∞ from 0.8 to 0.9 cm. Thus the pits formed by such chimneys appear to be too shallow to explain the present observations. The inference is that for this mechanism to apply, a different burrowing organism would be required.

[53] The low nucleus detection rate provides an additional limit on the probable size range of the obstacles. Assuming

the nuclei could have been hidden within the acoustic shadow cast by the near edge of the pit, the maximum size of an object hidden within a pit of diameter D would be given by

$$d_{ho} \simeq D(\tan \beta - \tan \phi(r, D))/2, \quad (12)$$

where d_{ho} is the diameter of the hidden obstacle, β and ϕ are the pit wall slope and grazing angle as before, and $\tan \phi = z_s/(r - D/2)$, r being the radial distance along the bottom from the sonar location to the pit center, and z_s the height of the sonar above bottom. Figure 18 shows d_{ho} over the range of r of interest for 5 representative pit diameters and a conservative value of β (25°). For $r > 2$ m, which represents 90% of the area of interest, the values of d_{ho} are 1–8 cm, or 5–15% of the pit diameter. Recalling that the pixel size in the sonar images is close to 1 cm on a side, and that several pixels would be needed to unambiguously identify a nucleus, larger objects partially protruding above the pit shadow zone would also go undetected. Thus objects 2–10 cm in diameter, or roughly 20% of their respective pit diameters, would likely not have been detected over most of the area of interest. This size range is consistent with the range of sizes of the possible objects mentioned above.

4.3. Other Possibilities

[54] There have been other studies of scour pits in shallow marine environments. *Reidenauer and Thistle* [1981] observed pits made by stingrays in fine sand in 2–3 m water depth with 30 cm median diameters, 6 cm scour depths, and 0.5 m^{-2} areal densities, characteristics all quite similar to the pits reported here. The *Reidenauer and Thistle* [1981] study site, however, was protected by barrier islands, conditions were calm with < 10 cm/s mean currents, and the pits lasted for at least 3 days. In contrast, the pits reported here occurred on the open coast under highly active sediment transport conditions in association with storms: ray pits seem an unlikely explanation. *de Boer* [1981] has shown that locally enhanced erosion can occur in the intertidal zone if the surficial layer of micro-organisms binding sand grains together is disrupted. While this mechanism might under some conditions lead to differential erosion and transport rates in the nearshore zone, it is difficult to envision it playing a role in the formation of the present scour pits which occurred after the evolution of the bed through a sequence of ripple types including flat bed, processes which would almost certainly have destroyed any microbially bound surficial sand layer.

[55] *Dorr and Kauffman* [1963] [see also *Allen*, 1984] reported finding “circular rippled depressions” below the low tide line in Cook Inlet, Alaska, and describe the depressions as being smaller but similar to those found around isolated cobbles on the nearby tidal flat, yet without a central obstacle. *Dorr and Kauffman* [1963] used this observation as evidence in support of their proposed mechanism for the formation of rippled toroids, a type of clast found in some sandstone beds of shallow water marine origin. According to *Dorr and Kauffman* [1963], rippled toroids range in size from 10 to 60 cm. They did not observe a central nucleus in any broken toroid, finding instead a low elevated cone of sand in the center of the depression. Based in part on laboratory experiments with vortex-generated

sand pits, they suggested that rippled toroids and the Cook Inlet pits were produced by vortices associated with rip currents or zones of horizontal shear in the longshore current. During the course of the present study, pit formation by vortex scour was one of the possibilities which we considered. We were initially unaware of the *Dorr and Kauffman* [1963] paper, our thinking being influenced instead by the *Nadaoka et al.* [1989] laboratory observations of obliquely descending vortices behind breaking waves. The vertical or oblique vortex mechanism is an intriguing possibility. For the present scour pits, however, the evidence overall, and in particular the clustering of pit occurrence locations, in our opinion favor the obstacle mechanism.

4.4. Speculative Remarks

[56] The hidden obstacle explanation for the observed low nucleus detection rate requires a mechanism whereby the nuclei “sink” below the level of the sand-water interface. Liquefaction is one possibility. Liquefaction occurs as a result of the buildup, either momentarily or progressively, of pore water pressure within the sediment. The physics of the liquefaction process, and the results from experimental studies of objects sinking into the seabed due to wave-forced liquefaction, are summarized by *Sumer and Fredsoe* [2002]. These experiments have been carried out mainly with models representing large relatively immobile objects, such as pipelines, armor blocks, or mines. While not discounting liquefaction as a potential mechanism, we would like to suggest the additional possibility that the $O(1)$ cm to $O(10)$ cm diameter obstacles being considered here may be small enough to be displaced by the fluid forcing, and that they may therefore actively participate in the scour process by either rolling or sliding. The necessary “sinking” could then result from the nucleus being pushed or rolled into the scour depression. Failure of the underlying soil might or might not accompany this process.

[57] Semimobile nuclei would also help to explain why most scour pits were short-lived (Figure 12), and why few pits developed into lunate megaripples. Perhaps the nucleus, being small, can either be swept out of the pit or pushed into the scour moat and then buried, after which the pit would decay due to the absence of a nucleus. Perhaps pits which lived longer and grew larger did so because their nuclei were larger and did not get swept away or buried. Since particle size spectra are generally red (i.e., smaller particles are more frequent), the relative rarity of large, long-lived scour pits would follow from the relative rarity of large nuclei. This line of reasoning also suggests that the infrequent development of scour pits into lunate megaripples might have been due, in part at least, to a dearth of sufficiently large obstacles.

5. Summary and Conclusions

[58] Results have been presented from the SandyDuck97 experiment which indicate the frequent occurrence of depressions in the sandy seafloor ≈ 30 cm in diameter and $O(10)$ cm deep. The depressions occurred over a relatively narrow range of wave energies ($u_{rms} = 0.32 \pm 0.05$ cm/s), and during both the wave growth and wave decay phases of all 13 forcing events captured in the 77 day data record. The

observations were made using rotary imaging sonars, mainly at two locations 40 m apart in the cross-shore direction in ≈ 3 m mean water depth. The depressions were sparsely distributed, with $O(0.1)$ m^{-2} mean areal number densities. Depressions were 6.5 times more frequent at the inner station ($N = 484$) than at the outer location ($N = 75$). At the inner station, depressions occurred twice as often as lunate megaripples, but with about the same frequency as lunate megaripples at the outer station. Depressions were also observed at a third location in the inner surf zone, though the data from this location are very limited.

[59] We conclude that the likely origin of the depressions is scour about compact obstacles on or embedded within the seabed. This conclusion is based on (1) the depths, diameters and growth rates being consistent with those predicted by relationships based on laboratory investigations of scour around vertical piles and short cylindrical objects; (2) the diameters being consistent with other observations in the nearshore of scour about rocks on a sand substrate; (3) the fact that the depressions sometimes formed on an otherwise featureless flat bed; (4) in the one instance for which compact obstacles (hydrozoan colony fragments) were known to be on the seabed, depressions formed about these objects; and (5) the spatial distribution of depression first occurrences was nonrandom, more than 50% instead occurring in approximately the same locations and resulting in a clustered, non-Poisson occurrence-location distribution.

[60] The nature of the obstacles is not clear. Stones and pebbles, known on the basis of sediment cores to occur in the study area, are one possibility. Large shells or shell fragments, also known to be present, represent another. Scour pits have also been previously observed in the inner surf zone, at a different location, around the chimney structures left by burrowing shrimp. The walls of such burrows therefore represent another possible obstacle type.

[61] In 13 instances, meter-scale lunate megaripples were observed to grow from these small initial depressions. The scour pits are therefore of much greater significance than their small initial sizes might otherwise suggest. Lunate megaripples represent a large-amplitude morphodynamic signal of considerable interest in the nearshore dynamics community. The results presented here indicate that these major roughness features can form from a compact initial pit. Conversely, since scour pits occurred more frequently than lunate megaripples, these same results indicate that the transformation from a pit to a megaripple is not always realized. The implications are that we need not only to identify those naturally occurring objects and/or processes which lead to pit formation, but also to understand what constitute the “right conditions” for the pit-to-megaripple transformation. We have speculated here that the right conditions likely involve the obstacle size: in particular, that there may be a minimum obstacle size (appropriately nondimensionalized) below which the associated scour pit does not develop into a lunate form.

[62] **Acknowledgments.** The authors thank the personnel at the FRF, and W. Birkemeier in particular, for their outstanding support during SandyDuck97. We also thank Wes Paul and Robert Craig, whose efforts in developing the hardware and software components of the rotary sonar data acquisition and control system were critical to the success of this project, Todd Mudge for assistance with the data processing, Tony Bowen

for the EM flowmeter and pressure sensor data, and the other members of the field team. Jon Grant and Peter Jumars provided valuable insight into the literature on biologically mediated scour pits. This research was supported by grants from the Collaborative Special Projects program of the Natural Sciences and Engineering Council of Canada and from the Coastal Sciences program of the U.S. Office of Naval Research.

References

- Allen, J. R. L. (1984), *Sedimentary Structures: Their Character and Physical Basis*, vol. 2, 2nd ed., 663 pp., Elsevier, New York.
- Birkemeier, W. A., H. C. Miller, S. D. Wilhelm, A. E. DeWall, and C. S. Gorbics (1985), A user's guide to the Coastal Engineering Center's (CERC's) Field Research Facility, *Tech. Rep. CERC-85-1*, 137 pp., Coastal Eng. Res. Cent. U.S. Army Corps of Eng., Vicksburg, Miss.
- Clifton, H. E. (1976), Wave-formed sedimentary structures—A conceptual model, in *Beach and Nearshore Sedimentation, Spec. Publ. 24*, edited by R. A. Davis Jr. and R. L. Ethington, pp. 126–148, Soc. for Sediment. Geol., Tulsa, Okla.
- de Boer, P. L. (1981), Mechanical effects of micro-organisms on intertidal bedform migration, *Sedimentology*, 28, 129–132.
- Dorr, J. A., Jr., and E. G. Kauffman (1963), Rippled toroids from the Napoleon Sandstone member (Mississippian) of southern Michigan, *J. Sediment. Petrol.*, 33, 751–758.
- Elgar, S. (1987), Relationships involving third moments and bispectra of a harmonic process, *IEEE Trans. Acoust. Speech Signal Processing*, 35, 1725–1726.
- Elgar, S., M. H. Freilich, and R. T. Guza (1990), Model-data comparisons of moments of nonbreaking shoaling surface gravity waves, *J. Geophys. Res.*, 95, 16,055–16,063.
- Feller, W. (1968), *An Introduction to Probability Theory and its Applications*, vol. 1, 3rd ed., 509 pp., John Wiley, Hoboken, N. J.
- Gallagher, E. L., S. Elgar, and E. D. Thornton (1998), Observations and predictions of megaripple migration in a natural surf-zone, *Nature*, 394, 165–168.
- Hay, A. E., and T. Mudge (2005), Principal bedstates during SandyDuck97: Occurrence, spectral anisotropy, and the bedstate storm cycle, *J. Geophys. Res.*, 110, C03013, doi:10.1029/2004JC002451.
- Hay, A. E., and D. L. Wilson (1994), Rotary sidescan images of nearshore bedform evolution during a storm, *Mar. Geol.*, 119, 57–65.
- Henderson, S. M., and A. J. Bowen (2002), Observations of surf beat forcing and dissipation, *J. Geophys. Res.*, 107(C11), 3193, doi:10.1029/2000JC000498.
- Herbich, J. B., R. E. Schiller Jr., R. K. Watanabe, and W. A. Dunlap (1984), *Seafloor Scour*, CRC Press, Boca Raton, Fla.
- Hill, G. W., and R. E. Hunter (1976), Interaction of biological and geological processes in the beach and nearshore environments, northern Padre Island, Texas, in *Beach and Nearshore Sedimentation, Spec. Publ. 24*, edited by R. A. Davis Jr. and R. L. Ethington, pp. 169–187, Soc. for Sediment. Geol., Tulsa, Okla.
- Nadaoka, K., M. Hino, and Y. Koyano (1989), Structure of the turbulent flow under breaking waves in the surf zone, *J. Fluid Mech.*, 204, 359–387.
- Ngusaru, A. S., and A. E. Hay (2004), Cross-shore migration of lunate megaripples during Duck94, *J. Geophys. Res.*, 109, C02006, doi:10.1029/2002JC001532.
- Nielsen, P. (1992), *Coastal Bottom Boundary Layers and Sediment Transport*, 324 pp., World Sci., Hackensack, N. J.
- Palmer, H. D. (1969), Wave-induced scour on the sea floor, in *Proceedings of Civil Engineering in the Oceans II*, pp. 703–713, Am. Soc. Civ. Eng., Reston, Va.
- Reidenaar, J. A., and D. Thistle (1981), Response of a soft-bottom hapacticoid community to stingray (*dasyatis sabina*) disturbance, *Mar. Biol.*, 65, 261–267.
- Schwartz, R. K., D. W. Cooper, and P. H. Etheridge (1997), Sedimentologic architecture of the shoreface prism, relationship to profile dynamics, and relevance to engineering concerns: Duck, North Carolina, *Tech. Rep. CHL-97*, USACE Waterw. Exper. Stat., Vicksburg, Miss.
- Sleath, J. F. A. (1984), *Sea Bed Mechanics*, John Wiley, Hoboken, N. J.
- Sumer, B. M., and J. Fredsoe (2001), Scour around pile in combined waves and current, *J. Hydrol. Eng.*, 127, 403–411.
- Sumer, B. M., and J. Fredsoe (2002), *The Mechanics of Scour in the Marine Environment*, 536 pp., World Sci., Hackensack, N. J.
- Thornton, E. B., and R. T. Guza (1983), Transformation of wave height distribution, *J. Geophys. Res.*, 88, 5925–5938.
- Voropayev, S. I., F. Y. Testik, H. J. S. Fernando, and D. L. Boyer (2003), Burial and scour around short cylinders under progressive shoaling waves, *Ocean Eng.*, 30, 1647–1667.

A. E. Hay and R. Speller, Department of Oceanography, Dalhousie University, Halifax, NS, Canada B3H 4J1. (alex.hay@dal.ca; rachel@coastalandoceans.com)